Journal of Computational Physics 347 (2017) 367–381

Contents lists available at ScienceDirect

Journal of Computational Physics

www.elsevier.com/locate/jcp

Unconditionally stable methods for gradient flow using Convex Splitting Runge–Kutta scheme

Jaemin Shin [a], Hyun Geun Lee [b], June-Yub Lee [c,*]

[a] Institute of Mathematical Sciences, Ewha Womans University, Seoul 03760, Republic of Korea
[b] Department of Mathematics, Kwangwoon University, Seoul 01897, Republic of Korea
[c] Department of Mathematics, Ewha Womans University, Seoul 03760, Republic of Korea

ARTICLE INFO

Article history:
Received 3 November 2016
Received in revised form 30 June 2017
Accepted 3 July 2017
Available online 10 July 2017

Keywords:
Gradient flow
Convex splitting
Gradient stability
Energy stability
Phase-field model
Cahn–Hilliard equation

ABSTRACT

We propose a Convex Splitting Runge–Kutta (CSRK) scheme which provides a simple unified framework to solve a gradient flow in an unconditionally gradient stable manner. The key feature of the scheme is a combination of a convex splitting method and a specially designed multi-stage two-additive Runge–Kutta method. Our methods are high order accurate in time and assure the gradient (energy) stability for any time step size. We provide detailed proof of the unconditional energy stability and present issues on the practical implementations. We demonstrate the accuracy and stability of the proposed methods using numerical experiments of the Cahn–Hilliard equation.

1. Introduction

Gradient systems have been fundamental in the development of many important concepts in dynamical systems [1]. In particular, gradient systems are important in many phenomenological models of phase transition such as the Allen–Cahn and Cahn–Hilliard equations [2,3]. We concentrate on a numerical method for solving the initial value problem, which can be represented as the gradient flow for $F : \mathbb{R}^N \to \mathbb{R}$,

$$\frac{\partial \phi}{\partial t} = -\text{grad}\, F(\phi), \tag{1}$$

where $\text{grad}\, F(\phi)$ is a gradient of F, $\phi(t) \in \mathbb{R}^N$, and N is the dimension of data space. It is worth noting that the energy function $F(\phi)$ is non-increasing in time since (1) is of gradient type.

$$\frac{d}{dt} F(\phi) = \left\langle \text{grad}\, F(\phi), \frac{\partial \phi}{\partial t} \right\rangle = -\|\text{grad}\, F(\phi)\|^2 \leq 0, \tag{2}$$

where $\langle \cdot, \cdot \rangle$ is an inner product on $\mathbb{R}^N$ with the corresponding norm $\|\phi\|^2 = \langle \phi, \phi \rangle$. Here, the gradient operator "grad" depends on the given inner product space. For example, Allen–Cahn and Cahn–Hilliard equations can be represented by gradient flows with the Ginzburg–Landau free energy functional under the L^2 and H^{-1} inner products, respectively.

* Corresponding author.
E-mail address: jyllee@ewha.ac.kr (J.-Y. Lee).

http://dx.doi.org/10.1016/j.jcp.2017.07.006
0021-9991/

Denoting ϕ^n as a numerical approximation of $\phi\left(t^n\right)$, we aim to develop a numerical method for one step evolution to obtain ϕ^{n+1} at $t^n + \Delta t$. A numerical integration method for (1) is said to be gradient stable [1,4] if a critical time step size Δt_c and a function $\mathcal{F}: \mathbb{R}^N \to \mathbb{R}$ exist such that:

$$\mathcal{F}(\phi) \geq 0 \text{ for all } \phi \in \mathbb{R}^N, \tag{3}$$

$$\mathcal{F}(\phi) \to \infty \text{ as } \|\phi\| \to \infty, \tag{4}$$

$$\mathcal{F}\left(\phi^{n+1}\right) \leq \mathcal{F}\left(\phi^n\right) \text{ for } \phi^n \in \mathbb{R}^N, \tag{5}$$

for all $0 < \Delta t \leq \Delta t_c$. We are particularly interested in unconditional stability which means that a method is stable no matter what a time step is taken. A method is said to be energy stable if it satisfies the energy dissipation property (5) and $\mathcal{F}$ may or may not be identical to the original energy function F.

It is numerically very important to use an unconditionally gradient (energy) stable method and this has been a serious research objective in the fields. For a convex F, finding an unconditionally gradient stable method is relatively easy since (1) is a contractive problem and the set of equilibria defines a convex set. However, many problems with a nonconvex F can have multiple isolated equilibria [4], and developing an unconditionally gradient (energy) stable method is a challenging task.

To solve the gradient flow with the nonconvex F, a convex splitting (CS) method was developed by Elliott and Stuart [5] and revitalized by the work of Eyre [6]. An energy function $F(\phi)$ is split into contractive and expansive parts, $F(\phi) = F_c(\phi) - F_e(\phi)$, where both $F_c(\phi)$ and $F_e(\phi)$ are convex. By treating $F_c(\phi)$ implicitly and $F_e(\phi)$ explicitly, the first order CS method is obtained by

$$\frac{\phi^{n+1} - \phi^n}{\Delta t} = -\text{grad}\, F_c\left(\phi^{n+1}\right) + \text{grad}\, F_e\left(\phi^n\right). \tag{6}$$

It is well known that the energy of the numerical solution of (6) monotonically decreases regardless of the time step size $\Delta t > 0$. Thus, (6) is said to be unconditionally gradient (energy) stable.

In general, many phase field equations can be modeled by gradient flows with a particular energy functional. Due to the nonlinearity of the energy functional as well as the high order differential terms, a severe stability restriction exists on the time step when applying typical numerical methods to the phase field equations. The first order and unconditionally gradient stable CS method, proposed for solving the Cahn–Hilliard equation [6], has affected many types of numerical methods for phase field equations. Semi-implicit methods such as the CS method improve the stability, however all semi-implicit methods do not guarantee the unconditional gradient stability as referred in [7].

While many researchers [8–11] have proposed higher order accurate methods, their methods do not guarantee unconditional energy stability. This is not a review paper but we would like to mention some of noteworthy researches related to second order energy stable methods. Recently, a number of significant second order convex splitting methods have been proposed considering the energy stability for a wide class of phase field model, such as Cahn–Hilliard [12,13], phase-field crystal [14–16], modified phase-field crystal [17], and epitaxial thin film growth [18,19] equations. Furthermore, the extensive works show that CS is available to the phase field models for the tumor growth [12] and polymer blend [20]. We should note that there have been another direction of the second order energy stable methods for various phase field model [21, 22], which is not extension of the CS idea.

Recently, we proposed a Convex Splitting Runge–Kutta (CSRK) scheme in [23], which combines the convex splitting strategy with the implicit–explicit (IMEX) Runge–Kutta (RK) method [24,25]. Since IMEX-RK methods have many choices for the coefficients of the RK tables, we were motivated to develop a high order accurate method with sufficient energy stability. We numerically demonstrated the improvement of the energy stability for solving the phase field equations using various types of CSRK methods. While numerical results indicate the notable improvement of the energy stability, we did not disclose the fundamental reasons why the stability was improved. Nonetheless, the previous study empirically suggests the likely existence of high order methods with the unconditional energy stability.

The object of this current paper is to show the existence of higher order unconditionally energy stable CSRK methods. In Section 2, we propose a two-additive RK method combined with a convex splitting strategy and a resemble condition, referred to as the CSRK-R method. In Section 3, we provide a sufficient condition to ensure the proposed method is unconditionally energy stable with detailed proof. In Section 4, for the practical implementations, we consider the IMEX-RK methods while guaranteeing the unique solvability. We also present a number of numerical methods that achieve the higher order of accuracy in time. In Section 5, we apply the proposed methods to the Cahn–Hilliard equation, which is a typical gradient flow in the phase field model. Finally, conclusions are drawn in Section 6. In the Appendix A, to ensure this article is self-contained, we briefly introduce the order conditions for the two-additive RK methods.

2. Convex Splitting Runge–Kutta methods with a resemble condition (CSRK-R)

First, we briefly review a two-additive RK method. In many applications, initial value problems can be given as additively partitioned systems,

$$\frac{\partial \phi}{\partial t} = f(\phi) + g(\phi) \text{ and } \phi(0) = \phi^0, \tag{7}$$

where the right-hand side is split into two different parts with respect to stiffness, nonlinearity, dynamical behavior, evaluation cost, etc. We refer to [25,26] for information on the case of more than two splitting systems. An additive scheme for (7) applies two different RK methods for each $f(\phi)$ and $g(\phi)$. We denote two s-stage RK tables in the Butcher notation

$$\begin{array}{c|c} \mathbf{c} & \mathbf{A} \\ \hline & \mathbf{b}^T \end{array} = \begin{array}{c|cccccc} 0 & 0 & 0 & 0 & \cdots & 0 \\ c_1 & a_{10} & a_{11} & a_{12} & \cdots & a_{1s} \\ c_2 & a_{20} & a_{21} & a_{22} & \cdots & a_{2s} \\ \vdots & \vdots & \vdots & \vdots & \ddots & \vdots \\ c_s & a_{s0} & a_{s1} & a_{s2} & \cdots & a_{ss} \\ \hline & b_0 & b_1 & b_2 & \cdots & b_s \end{array}, \quad \begin{array}{c|c} \hat{\mathbf{c}} & \hat{\mathbf{A}} \\ \hline & \hat{\mathbf{b}}^T \end{array} = \begin{array}{c|cccccc} 0 & 0 & 0 & 0 & \cdots & 0 \\ \hat{c}_1 & \hat{a}_{10} & \hat{a}_{11} & \hat{a}_{12} & \cdots & \hat{a}_{1s} \\ \hat{c}_2 & \hat{a}_{20} & \hat{a}_{21} & \hat{a}_{22} & \cdots & \hat{a}_{2s} \\ \vdots & \vdots & \vdots & \vdots & \ddots & \vdots \\ \hat{c}_s & \hat{a}_{s0} & \hat{a}_{s1} & \hat{a}_{s2} & \cdots & \hat{a}_{ss} \\ \hline & \hat{b}_0 & \hat{b}_1 & \hat{b}_2 & \cdots & \hat{b}_s \end{array}. \tag{8}$$

where $\mathbf{A}, \hat{\mathbf{A}} \in \mathbb{R}^{(s+1)\times(s+1)}$, $\mathbf{b}, \hat{\mathbf{b}} \in \mathbb{R}^{s+1}$, and the coefficients $\mathbf{c}$ and $\hat{\mathbf{c}}$ are usually given by $\mathbf{c} = \mathbf{A}\mathbf{1}$ and $\hat{\mathbf{c}} = \hat{\mathbf{A}}\mathbf{1}$, respectively, with $\mathbf{1} = (1, 1, \ldots, 1)^T \in \mathbb{R}^{s+1}$.

With the Butcher tables (8), the time marching algorithm can be written as follows: We denote ϕ^n as an approximation of $\phi(t^n)$. With a time step size Δt, one step evolution from t^n to $t^{n+1} = t^n + \Delta t$ of the additive RK method is given as follows. Given ϕ^n, we will calculate the next time approximation ϕ^{n+1} with the intermediate stages, $\phi_0, \phi_1, \cdots, \phi_s$. We set a zero-stage as $k_0 = f(\phi_0)$ and $\hat{k}_0 = g(\phi_0)$, where $\phi_0 = \phi^n$. For each stage $i = 1, 2, \ldots, s$, we calculate

$$\phi_i = \phi_0 + \Delta t \left(\sum_{j=0}^{s} a_{ij} k_j + \sum_{j=0}^{s} \hat{a}_{ij} \hat{k}_j \right), \tag{9}$$

where $k_i = f(\phi_i)$ and $\hat{k}_i = g(\phi_i)$. Here, ϕ_i is the approximation of $\phi(t^n + c_i \Delta t)$ on the i-th stage. In addition, we evaluate the next time approximation ϕ^{n+1} as

$$\phi^{n+1} = \phi_0 + \Delta t \sum_{j=0}^{s} \left(b_j k_j + \hat{b}_j \hat{k}_j \right). \tag{10}$$

In the Appendix A, we describe the order conditions of the two-additive RK method up to third order accuracy.

We now introduce a new class of CSRK method with the additional design criterion called the *resemble condition*, which plays a key role in the development of energy stable methods. We start by considering two conditions as follows.

Condition 1 *(Resemble condition). For the Butcher notations in (8),* $\mathbf{A}$ *and* $\hat{\mathbf{A}}$ *are said to be satisfying the resemble condition if* $\hat{\mathbf{A}} = \mathbf{A}S$*, where* $S_{ij} = \delta_{i,j+1}$ *is a shift matrix and* δ_{ij} *is the Kronecker delta symbol.*

Condition 2 *(Stiffly accurate condition). For the Butcher notations in (8),* $\mathbf{A}$*,* $\mathbf{b}$ *and* $\hat{\mathbf{A}}$*,* $\hat{\mathbf{b}}$ *are said to be satisfying the stiffly accurate condition if* $b_j = a_{sj}$ *and* $\hat{b}_j = \hat{a}_{sj}$ *for* $j = 0, 1, \ldots, s$*.*

To be satisfied the condition 1, $\mathbf{A}$ and $\hat{\mathbf{A}}$ should be constructed as

$$\mathbf{A} = \begin{pmatrix} 0 & \mathbf{0}^T \\ \mathbf{0} & \mathbf{R} \end{pmatrix}, \quad \hat{\mathbf{A}} = \begin{pmatrix} \mathbf{0}^T & 0 \\ \mathbf{R} & \mathbf{0} \end{pmatrix}, \tag{11}$$

where we denote as a resemble base matrix $\mathbf{R}$,

$$\mathbf{R} = \begin{pmatrix} r_{11} & \cdots & r_{1s} \\ \vdots & \ddots & \vdots \\ r_{s1} & \cdots & r_{ss} \end{pmatrix}. \tag{12}$$

Therefore, the condition 1 automatically implies that the (canopy node) condition $\mathbf{c} = \hat{\mathbf{c}}$. In addition, the condition 2 is motivated because it is known that an A-stable RK method is L-stable if $b_j = a_{sj}$ [27]. With the conditions 1 and 2, we consider the s-stage resemble RK table only with a resemble base matrix $\mathbf{R}$

$$\begin{array}{c|c} \mathbf{c} & \mathbf{A} \\ \hline & \mathbf{b}^T \end{array} = \begin{array}{c|cccc} 0 & 0 & 0 & \cdots & 0 \\ c_1 & 0 & r_{11} & r_{12} & \cdots & r_{1s} \\ c_2 & 0 & r_{21} & r_{22} & \cdots & r_{2s} \\ \vdots & \vdots & \vdots & \vdots & \ddots & \vdots \\ c_s & 0 & r_{s1} & r_{s2} & \cdots & r_{ss} \\ \hline & 0 & r_{s1} & r_{s2} & \cdots & r_{ss} \end{array}, \quad \begin{array}{c|c} \hat{\mathbf{c}} & \hat{\mathbf{A}} \\ \hline & \hat{\mathbf{b}}^T \end{array} = \begin{array}{c|cccc} 0 & 0 & 0 & 0 & \cdots & 0 \\ c_1 & r_{11} & r_{12} & r_{13} & \cdots & 0 \\ c_2 & r_{21} & r_{22} & r_{23} & \cdots & 0 \\ \vdots & \vdots & \vdots & \vdots & \ddots & \vdots \\ c_s & r_{s1} & r_{s2} & \cdots & r_{ss} & 0 \\ \hline & r_{s1} & r_{s2} & \cdots & r_{ss} & 0 \end{array} \tag{13}$$

Using the conditions 1 and 2, we can describe the resemble RK method (13) only using a resemble base matrix $\mathbf{R}$. Furthermore, by condition 2, the time evaluation (10) is reduced to $\phi^{n+1} = \phi_s$.

We now propose the s-stage CSRK methods with the resemble condition (CSRK-R). First, we recall the convex splitting (CS) method (6) for

$$\frac{\partial \phi}{\partial t} = -\text{grad}\,(F_c(\phi) - F_e(\phi)) \tag{14}$$

can be written as

$$\phi_1 = \phi_0 - \Delta t\,\text{grad}\,(F_c(\phi_1) - F_e(\phi_0))\,, \tag{15}$$

where $\phi_0 = \phi^n$ and $\phi_1 = \phi^{n+1}$. We can represent (15) as the framework of the resemble RK method with a trivial resemble base matrix $\mathbf{R} = (1)$ by defining $f(\phi) = -\text{grad}\,F_c(\phi)$ and $g(\phi) = \text{grad}\,F_e(\phi)$.

We now define the p-th order s-stage CSRK-R(p) methods by combining the CS scheme and the p-th order accurate resemble RK method (13). Let us consider a general resemble base matrix $\mathbf{R}$ with s-stages. To evaluate one time step, we set $\phi_0 = \phi^n$ and estimate

$$\phi_i = \phi_0 - \Delta t \sum_{j=1}^{s} r_{ij}\,\text{grad}\left(F_c\left(\phi_j\right) - F_e\left(\phi_{j-1}\right)\right), \tag{16}$$

for $i = 1, 2, \ldots, s$ and we have $\phi^{n+1} = \phi_s$.

3. Unconditional energy stability requirement of CSRK-R

We give a single lemma before we present a condition to make the proposed CSRK-R scheme (16) unconditionally energy stable.

Lemma 1. *Suppose that ϕ and ψ are sufficiently regular and $F(\phi)$ is two times continuously differentiable. Consider the canonical convex splitting of $F(\phi)$ into $F(\phi) = F_c(\phi) - F_e(\phi)$; i.e. both $F_c(\phi)$ and $F_e(\phi)$ are convex, then*

$$F(\phi) - F(\psi) \le \langle \text{grad}\,F_c(\phi) - \text{grad}\,F_e(\psi)\,, \phi - \psi \rangle\,. \tag{17}$$

Proof. The analogous proof could be found in [14], however we introduce it for a self-contained description. Since $F_c(\phi)$ and $F_e(\phi)$ are convex,

$$F_c(\phi) - F_c(\psi) \le \langle \text{grad}\,F_c(\phi)\,, \phi - \psi \rangle\,, \tag{18}$$

$$F_e(\phi) - F_e(\psi) \ge \langle \text{grad}\,F_e(\psi)\,, \phi - \psi \rangle\,. \tag{19}$$

Using two inequalities,

$$\begin{aligned} F(\phi) - F(\psi) &= (F_c(\phi) - F_e(\phi)) - (F_c(\psi) - F_e(\psi)) \\ &\le \langle \text{grad}\,F_c(\phi)\,, \phi - \psi \rangle - \langle \text{grad}\,F_e(\psi)\,, \phi - \psi \rangle \\ &= \langle \text{grad}\,F_c(\phi) - \text{grad}\,F_e(\psi)\,, \phi - \psi \rangle\,. \qquad \square \end{aligned} \tag{20}$$

Condition 3 *(Positive definite condition). The CSRK-R method defined in (16) is said to be satisfying the positive definite condition if a row difference matrix $\widetilde{\mathbf{R}}$ is positive definite after a symmetric transformation, where $\widetilde{\mathbf{R}} = \mathbf{R} - S\mathbf{R}$ is defined as follows with a shift matrix $S_{ij} = \delta_{i,j+1}$,*

$$\widetilde{\mathbf{R}} = \begin{pmatrix} \tilde{r}_{11} & \tilde{r}_{12} & \cdots & \tilde{r}_{1s} \\ \tilde{r}_{21} & \tilde{r}_{22} & \cdots & \tilde{r}_{2s} \\ \vdots & \vdots & \ddots & \vdots \\ \tilde{r}_{s1} & \tilde{r}_{s2} & \cdots & \tilde{r}_{ss} \end{pmatrix} = \begin{pmatrix} r_{11} & r_{12} & \cdots & r_{1s} \\ r_{21} & r_{22} & \cdots & r_{2s} \\ \vdots & \vdots & \ddots & \vdots \\ r_{s1} & r_{s2} & \cdots & r_{ss} \end{pmatrix} - \begin{pmatrix} 0 & 0 & \cdots & 0 \\ r_{11} & r_{12} & \cdots & r_{1s} \\ \vdots & \vdots & \ddots & \vdots \\ r_{s-1,1} & r_{s-1,2} & \cdots & r_{s-1,s} \end{pmatrix}. \tag{21}$$

Theorem 2 *(Unconditional energy stability). Suppose that the row difference matrix* $\widetilde{\mathbf{R}}$ *is positive definite. The proposed CSRK-R scheme (16) is then unconditionally energy stable, meaning that for any time step size* $\Delta t > 0$,

$$F\left(\phi^{n+1}\right) \leq F\left(\phi^{n}\right). \tag{22}$$

Proof. For simple description, we define the difference operator by $[\![\phi]\!]_m^n = \phi_n - \phi_m$ and the auxiliary variable by $G_j = F_c\left(\phi_j\right) - F_e\left(\phi_{j-1}\right)$. Then, we can rewrite (16) as

$$[\![\phi]\!]_0^i = -\Delta t \sum_{j=1}^{s} r_{ij} \operatorname{grad} G_j, \tag{23}$$

for $i = 1, 2, \ldots, s$. The difference between the two adjacent stages can be calculated as

$$[\![\phi]\!]_{i-1}^i = [\![\phi]\!]_0^i - [\![\phi]\!]_0^{i-1} = -\Delta t \sum_{j=1}^{s} \tilde{r}_{ij} \operatorname{grad} G_j, \tag{24}$$

for all i. By Lemma 1, the energy difference between two adjacent stages is

$$[\![F(\phi)]\!]_{i-1}^i \leq \left\langle \operatorname{grad} F_c\left(\phi_i\right) - \operatorname{grad} F_e\left(\phi_{i-1}\right), [\![\phi]\!]_{i-1}^i \right\rangle = \left\langle \operatorname{grad} G_i, [\![\phi]\!]_{i-1}^i \right\rangle. \tag{25}$$

After summing up, we have

$$[\![F(\phi)]\!]_0^s = \sum_{i=1}^{s} [\![F(\phi)]\!]_{i-1}^i \leq \sum_{i=1}^{s} \left\langle \operatorname{grad} G_i, [\![\phi]\!]_{i-1}^i \right\rangle = -\Delta t \left\langle \operatorname{grad} \mathbf{G}, \widetilde{\mathbf{R}} \operatorname{grad} \mathbf{G} \right\rangle_s, \tag{26}$$

where $\operatorname{grad} \mathbf{G} = (\operatorname{grad} G_1, \cdots, \operatorname{grad} G_s)^T$ and we define an s-dimensional inner product as $\langle \boldsymbol{\phi}, \boldsymbol{\psi} \rangle_s = \sum_{i=1}^{s} \langle \phi_i, \psi_i \rangle$ for $\boldsymbol{\phi} = (\phi_1, \cdots, \phi_s)^T$ and $\boldsymbol{\psi} = (\psi_1, \cdots, \psi_s)^T$. Since $\widetilde{\mathbf{R}}$ is positive definite, $[\![F(\phi)]\!]_0^s \leq 0$. It follows that the energy dissipation $F\left(\phi^{n+1}\right) = F\left(\phi_s\right) \leq F\left(\phi_0\right) = F\left(\phi^n\right)$. □

Finally, we could design an energy stable method for the CSRK-R methods using only the positive definiteness condition of $\widetilde{\mathbf{R}}$. The three sufficient conditions play an important role in the CSRK method in being unconditionally energy stable. Note that this development provides the possibility of existing conditions or designs to guarantee the energy stability.

4. Implementations of unconditionally energy stable CSRK-R method

A simple choice for CSRK-R is to consider the type of implicit–explicit Runge–Kutta (IMEX-RK) method which applies an implicit discretization to one term and an explicit discretization to the other term. A method with a full matrix in (13) requires the solution of s simultaneous implicit (in general nonlinear) equations per step. To circumvent this difficulty, a lower triangular matrix could be suggested. Then we just need to solve a single implicit equation for each stage, which is motivated by "diagonally implicit" RK method [28]. This means that, in CSRK-R, we select a lower triangular type for the resemble base matrix

$$\mathbf{R} = \begin{pmatrix} r_{11} & 0 & \cdots & 0 \\ r_{21} & r_{22} & \cdots & 0 \\ \vdots & \vdots & \ddots & \vdots \\ r_{s1} & r_{s2} & \cdots & r_{ss} \end{pmatrix}. \tag{27}$$

With the resemble base matrix (27), the resemble RK method (13) is then reduced as follows:

$$\begin{array}{c|c} \mathbf{c} & \mathbf{A} \\ \hline & \mathbf{b}^T \end{array} = \begin{array}{c|cccccc} 0 & 0 & 0 & 0 & \cdots & 0 \\ c_1 & 0 & r_{11} & 0 & \cdots & 0 \\ c_2 & 0 & r_{21} & r_{22} & \cdots & 0 \\ \vdots & \vdots & \vdots & \vdots & \ddots & \vdots \\ c_s & 0 & r_{s1} & r_{s2} & \cdots & r_{ss} \\ \hline & 0 & r_{s1} & r_{s2} & \cdots & r_{ss} \end{array}, \quad \begin{array}{c|c} \hat{\mathbf{c}} & \hat{\mathbf{A}} \\ \hline & \hat{\mathbf{b}}^T \end{array} = \begin{array}{c|cccccc} 0 & 0 & 0 & 0 & \cdots & 0 \\ c_1 & r_{11} & 0 & 0 & \cdots & 0 \\ c_2 & r_{21} & r_{22} & 0 & \cdots & 0 \\ \vdots & \vdots & \vdots & \vdots & \ddots & \vdots \\ c_s & r_{s1} & r_{s2} & \cdots & r_{ss} & 0 \\ \hline & r_{s1} & r_{s2} & \cdots & r_{ss} & 0 \end{array}. \tag{28}$$

As (16) comes from (13), we can derive the following scheme from (28). First, we set a zero-stage as $k_0 = -\operatorname{grad} F_c\left(\phi_0\right)$ and $\hat{k}_0 = \operatorname{grad} F_e\left(\phi_0\right)$, where $\phi_0 = \phi^n$. For each stage $i = 1, 2, \ldots, s$, we calculate

Table 1
Order conditions of two-additive RK methods up to the third order accuracy.

Order	Stand-alone conditions		Coupling conditions
1	$\mathbf{b}\cdot\mathbf{1}=1$	$\hat{\mathbf{b}}\cdot\mathbf{1}=1$	–
2	$\mathbf{b}\cdot\mathbf{c}=1/2$	$\hat{\mathbf{b}}\cdot\mathbf{c}=1/2$	–
3	$\mathbf{b}\cdot\mathbf{c}^2=1/3$	$\hat{\mathbf{b}}\cdot\mathbf{c}^2=1/3$	$\mathbf{b}\cdot\hat{\mathbf{A}}\mathbf{c}+\hat{\mathbf{b}}\cdot\mathbf{A}\mathbf{c}=1/3$
	$\mathbf{b}\cdot\mathbf{A}\mathbf{c}=1/6$	$\hat{\mathbf{b}}\cdot\hat{\mathbf{A}}\mathbf{c}=1/6$	

$$\phi_i=\phi_0+\Delta t\left(\sum_{j=1}^{i}r_{ij}k_j+\sum_{j=0}^{i-1}r_{i,j+1}\hat{k}_j\right), \tag{29}$$

where $k_i=-\operatorname{grad}F_c(\phi_i)$ and $\hat{k}_i=\operatorname{grad}F_e(\phi_i)$. Finally, we evaluate the next time approximation as $\phi^{n+1}=\phi_s$.

Theorem 3 *(Unique solvability). The proposed CSRK-R scheme (29) is uniquely solvable for any time step size $\Delta t>0$, provided that $r_{ii}\geq 0$ for all i.*

Proof. For each stage $i=1,2,\cdots,s$ of (29), we need to solve

$$\phi_i+r_{ii}\Delta t\operatorname{grad}F_c(\phi_i)=S_i, \tag{30}$$

where

$$S_i=\phi_0-\Delta t\left(\sum_{j=1}^{i-1}r_{ij}\operatorname{grad}F_c(\phi_j)-\sum_{j=0}^{i-1}r_{i,j+1}\operatorname{grad}F_e(\phi_j)\right). \tag{31}$$

Since F_c is convex, the function

$$Q(\phi)=\frac{1}{2}\|\phi\|^2+r_{ii}\Delta tF_c(\phi)-\langle\phi,S_i\rangle \tag{32}$$

has a unique minimization for any time step size $\Delta t>0$. At the unique minimizer for each stage, $\operatorname{grad}Q(\phi)=0$ and (30) has a unique solution ϕ_i. Therefore, the proposed scheme (29) is uniquely solvable for any time step size $\Delta t>0$. □

Remark 1. The s-stage CSRK-R defined in (29) requires the s inversions per step like (30), while one inversion is needed to solve some of existing second order convex splitting methods.

We now introduce some examples for the resemble base matrix $\mathbf{R}$ so that $\widetilde{\mathbf{R}}$ is positive definite. Of course, $\mathbf{A}$ and $\hat{\mathbf{A}}$ made from a given resemble base matrix $\mathbf{R}$ should satisfy the order conditions. We have $\mathbf{c}$ and $\hat{\mathbf{c}}$ by the usual relations $\mathbf{c}=\mathbf{A1}$ and $\hat{\mathbf{c}}=\hat{\mathbf{A}}\mathbf{1}$, respectively. By condition 2, we reconstruct $\mathbf{b}$ and $\hat{\mathbf{b}}$ from $\mathbf{A}$ and $\hat{\mathbf{A}}$, respectively. Condition 1 automatically implies that $\mathbf{c}=\hat{\mathbf{c}}$, and it reduces the massive order conditions listed in the Appendix A (Table 2); the reduced conditions are listed in Table 1. Obviously, the conditions 1 and 2 imply that the two order conditions $\mathbf{b}\cdot\mathbf{1}=1$ and $\hat{\mathbf{b}}\cdot\mathbf{1}=1$ are identical. We have 1 condition for the first order accuracy, 3 conditions for the second order accuracy, and 8 conditions for the third order accuracy.

In addition, for convenient design of the tables, we consider a singly diagonal matrix, i.e. $r_{ii}=\gamma$, for $i=1,2,\ldots,s$. For the first order accuracy, a resemble base matrix $\mathbf{R}$ is

$$\mathbf{R}=\begin{pmatrix}1\end{pmatrix}. \tag{33}$$

It is easy to show that (33) constructs a well-known CS method. For the second order accuracy, CSRK-R(2), a possible choice of resemble base matrix $\mathbf{R}$ is

$$\mathbf{R}=\begin{pmatrix}\frac{2}{3}&0&0\\-\frac{7}{12}&\frac{2}{3}&0\\-\frac{1}{3}&\frac{2}{3}&\frac{2}{3}\end{pmatrix}. \tag{34}$$

The positive definiteness of $\widetilde{\mathbf{R}}$ is easily shown by evaluating the all eigenvalues of $\left(\widetilde{\mathbf{R}}+\widetilde{\mathbf{R}}^T\right)/2$ are positive. For (34), the eigenvalues of $\left(\widetilde{\mathbf{R}}+\widetilde{\mathbf{R}}^T\right)/2$ are 0.0293, 0.6667, and 1.3040. For the third order accuracy, a possible choice of resemble base matrix $\mathbf{R}$ is

$$\mathbf{R}=\begin{pmatrix} \frac{1}{2} & 0 & 0 & 0 & 0 & 0 \\ \frac{1}{2} & \frac{1}{2} & 0 & 0 & 0 & 0 \\ -\frac{1}{10} & \frac{1}{10} & \frac{1}{2} & 0 & 0 & 0 \\ a_{41} & a_{42} & a_{43} & \frac{1}{2} & 0 & 0 \\ a_{51} & a_{52} & a_{53} & \frac{1}{20} & \frac{1}{2} & 0 \\ a_{61} & a_{62} & a_{63} & a_{64} & a_{65} & \frac{1}{2} \end{pmatrix}, \tag{35}$$

where

$$a_{41}=\frac{13252051}{50981620}, \quad a_{42}=-\frac{100507933}{407852960}, \quad a_{43}=\frac{19290953}{81570592}, \quad a_{51}=\frac{401851541}{5098162000},$$
$$a_{52}=-\frac{20327867}{637270250}, \quad a_{53}=-\frac{200790581}{1019632400}, \quad a_{61}=\frac{3217}{14300}, \quad a_{62}=-\frac{703}{7150},$$
$$a_{63}=-\frac{6359}{42900}, \quad a_{64}=-\frac{4556}{10725}, \quad a_{65}=\frac{406}{429}.$$

For (35), the eigenvalues of $\left(\widetilde{\mathbf{R}}+\widetilde{\mathbf{R}}^T\right)/2$ are 0.0063, 0.1105, 0.3582, 0.5722, 0.9225, and 1.0303. Therefore, we can say that our methods made by (34) and (35) satisfy the condition 3 and it is easy to check that the coefficients induced by those matrices satisfy the order conditions in Table 1.

Remark 2. The examples (34) and (35) show that the desired methods do indeed exist, which are the IMEX-RK methods with some special conditions. For interested readers on the construction of tables, we note that no 2-stage resemble RK method exists for the second order accuracy. Furthermore, the finding of the resemble RK methods for the third order accuracy with less than 6 stages is open.

Remark 3. We only consider up to the third order, because the object of this paper is to show the existence of the unconditionally gradient stable methods with the sufficient high order accuracy in time. Finding higher order methods appears to be rather tedious and could be somewhat difficult without some type of simplifying assumptions.

5. Numerical examples with Cahn–Hilliard equation

In this section, we apply the proposed CSRK-R method to the Cahn–Hilliard (CH) equation to numerically demonstrate that the method achieves high order accuracy and energy stability. Because of the high derivative term and the nonlinear term, which introduce a severe time step restriction for stability, the CH equation is a good example to demonstrate the applicability of the proposed methods. To the best of our knowledge, no third order method guaranteeing the unconditional gradient stability has been proposed to date.

For the order parameter ϕ, the Ginzburg–Landau free energy functional is given by

$$\mathcal{E}(\phi)=\int_{\Omega}\left(\Psi(\phi)+\frac{\epsilon^2}{2}|\nabla\phi|^2\right)d\mathbf{x}, \tag{36}$$

where Ω is a domain in $\mathbb{R}^d$ $(d=1,2,3)$, $\Psi(\phi)$ is a bulk free energy with two minima corresponding to the two phases, and $\epsilon>0$ is a parameter related to the interfacial thickness. For simplicity, we consider the polynomial free energy $\Psi(\phi)=\frac{1}{4}\left(\phi^2-1\right)^2$. We note that the energy functional (3) satisfies the conditions (3) and (4), so that combining with the CSRK-R method guaranteeing energy stability (5) provides a gradient stable method.

We consider the Hilbert space H_0 as a zero average space. For given $v_1, v_2 \in H_0$, we define the inner product of the dual space by $(v_1,v_2)_{H^{-1}}=\left(\nabla\varphi_{v_1},\nabla\varphi_{v_2}\right)_{L^2}$, where $\varphi_{v_1},\varphi_{v_2}\in H_0$ are the solutions of the homogeneous Neumann boundary value problems $-\Delta\varphi_{v_1}=v_1$ and $-\Delta\varphi_{v_2}=v_2$ in Ω. From the above definition, if $\psi\in H_0$, then we have the identity

$$(-\Delta\phi,\psi)_{H^{-1}}=(\phi,\psi)_{L^2}. \tag{37}$$

The CH equation is derived by the gradient flow with the Ginzburg–Landau free energy functional (36) under the H^{-1} inner product

$$\frac{\partial\phi}{\partial t}=-\mathrm{grad}_{H^{-1}}\mathcal{E}(\phi)=\Delta\left(\Psi'(\phi)-\epsilon^2\Delta\phi\right), \tag{38}$$

where

$$\left(\mathrm{grad}_{H^{-1}}\mathcal{E}(\phi),v\right)_{H^{-1}}=\left.\frac{d}{d\theta}\mathcal{E}(\phi+\theta v)\right|_{\theta=0}=\left(\Psi'(\phi)-\epsilon^2\Delta\phi,v\right)_{L_2}=\left(-\Delta\left(\Psi'(\phi)-\epsilon^2\Delta\phi\right),v\right)_{H^{-1}}. \tag{39}$$

To obtain the energy stable method, Eyre [29] developed the first order nonlinear CS method for the CH equation as

$$\frac{\phi^{n+1}-\phi^n}{\Delta t} = \Delta\left(\left(\phi^{n+1}\right)^3 - \epsilon^2\Delta\phi^{n+1} - \phi^n\right). \tag{40}$$

In this method, $\mathcal{E}(\phi)$ is split into a contractive part and an expansive part: $\mathcal{E}(\phi) = \mathcal{E}_c(\phi) - \mathcal{E}_e(\phi)$ where

$$\mathcal{E}_c(\phi) = \int_\Omega \left(\frac{1}{4}\phi^4 + \frac{1}{4} + \frac{\epsilon^2}{2}|\nabla\phi|^2\right) d\mathbf{x}, \quad \mathcal{E}_e(\phi) = \int_\Omega \frac{1}{2}\phi^2\, d\mathbf{x}. \tag{41}$$

And $\mathcal{E}_c(\phi)$ is treated implicitly, whereas $\mathcal{E}_e(\phi)$ is treated explicitly. It is easy to show that both $\mathcal{E}_c(\phi)$ and $\mathcal{E}_e(\phi)$ are convex. Now, we can construct the numerical method using the splitting (41) and s-stage CSRK-R(p) method (29) in Section 4. Given the resemble base matrix $\mathbf{R}$ with s-stages and desired order of accuracy, we evaluate one time step as follows: we set $\phi_0 = \phi^n$ and evaluate

$$\frac{\phi_i - \phi_0}{\Delta t} = \sum_{j=1}^{i} r_{ij}\Delta\left(\left(\phi_j\right)^3 - \epsilon^2\Delta\phi_j - \phi_{j-1}\right), \tag{42}$$

for $i = 1, 2, \ldots, s$ and we have $\phi^{n+1} = \phi_s$. To solve the i-th stage evaluation (42), we use a nonlinear iterative method with a Newton-type linearization of $(\phi_i)^3$. We refer to [16,30] for details of the nonlinear iterative solver.

Remark 4. As we introduce in (38), the CH equation is one of gradient flows under the H^{-1} inner product. Intuitively, the gradient in H^{-1} can be considered as $\text{grad}_{H^{-1}} = -\Delta\frac{\delta}{\delta\phi}$, where $\frac{\delta}{\delta\phi}$ is the functional derivative. Therefore, the unconditional energy stability and unique solvability of (42) are guaranteed by Theorem 2 and 3 with the resemble base matrices introduced in Section 4.

Remark 5. We apply a nonlinear convex splitting (41) to construct a CSRK-R method, so that the nonlinear systems (42) are obtained. However, it is just an example to show the applicability of CSRK-R methods. We can make a linear CSRK-R method by considering the linear convex splitting for (36). We refer to [23] for interested readers.

We now present examples to numerically demonstrate the accuracy and stability of the proposed method, CSRK-R(p), corresponding to the first order method (33), second order method (34), and third order method (35).

5.1. Solution evolution with random initial data in 1D

We begin by showing the solution evolution of the CH equation with the zero Neumann boundary condition and the randomly perturbed initial condition

$$\phi(x, 0) = 0.01 \cdot \text{rand}(x) \tag{43}$$

on a domain $\Omega = [0, 1]$, where the random number $\text{rand}(x)$ is uniformly distributed between -1 and 1. For the numerical simulations, $\epsilon = 0.02$ is used and the grid size is fixed at $\Delta x = 1/128$ which provides sufficient spatial accuracy. The numerical solution is evolved to time $T_f = 0.08$. We remark that spectral methods are used for spatial derivatives in the numerical computations. Simulations are executed by using the MATLAB program with a fast Fourier transform.

Fig. 1 shows the time evolution of the solution with a sufficiently small time step $\Delta t = T_f/2^{17}$ using the third order method CSRK-R(3). At the early stage, solutions are rearranged and adjusted to find their desired mode with low magnitude. After finishing the adjustment, the solution matures and approaches the steady-state solution. These solutions will be used as the reference solution to estimate the convergence rate in Section 5.2.

Fig. 2 shows the time evolution of free energy functional $\mathcal{E}(\phi)$ corresponding to the solution in Fig. 1. The property of the energy dissipation is validated and energy transitions are observed. The evolution will be used as the reference to compare with the energy evolution in Section 5.3.

5.2. Numerical convergence test with random initial data in 1D

We demonstrate the numerical convergence using the same conditions and parameters as those used in the previous section. To estimate the convergence rate with respect to a time step Δt, simulations are performed by varying the time steps $\Delta t = T_f/2^{15}, T_f/2^{14}, \ldots, T_f/2^3$.

Fig. 3 shows the relative l_2-errors of $\phi(x, t)$ with various time steps. Here, the errors are computed by comparison with the reference solution. It is observed that the CSRK-R(p) methods give the desired p-th order accuracy in time.

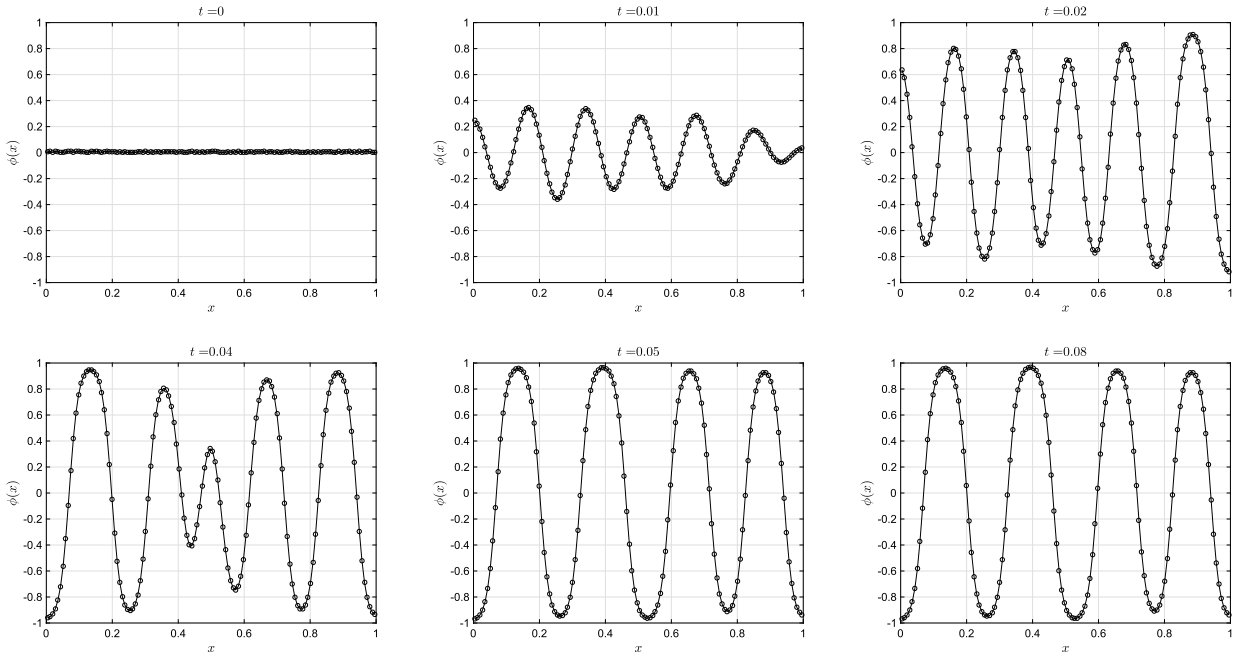

Fig. 1. Time evolution of solution for the CH equation in 1D.

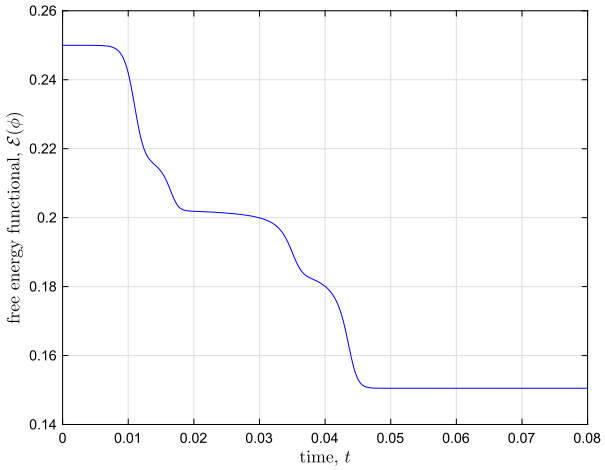

Fig. 2. Energy evolution for the CH equation in 1D.

5.3. Energy stability performance with random initial data in 1D

We display the energy evolutions with the same conditions and parameters as those used in the previous section. Simulations are performed by relatively large time steps $\Delta t = T_f/2^7, T_f/2^5, T_f/2^3$.

Fig. 4 shows the energy evolution with large time steps and the energy dissipations are observed for all simulations.

5.4. Solution evolution with random initial data in 2D

Next, we display the solution evolution of the CH equation with the zero Neumann boundary condition and the randomly perturbed initial condition

$$\phi(x, y, 0) = 0.001 \cdot \text{rand}(x, y) \tag{44}$$

on a domain $\Omega = [0, 1] \times [0, 1]$. For the numerical simulations, $\epsilon = 0.02$ is used and the grid size is fixed at $\Delta x = \Delta y = 1/512$. The numerical solution is evolved to time $T_f = 0.08$.

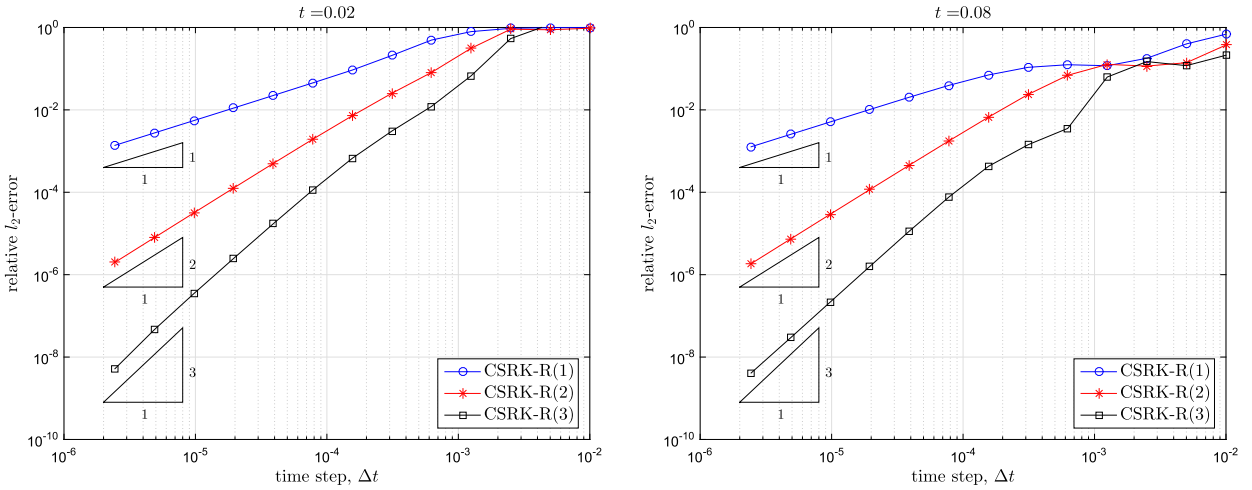

Fig. 3. Relative l_2-errors for various time steps Δt in 1D.

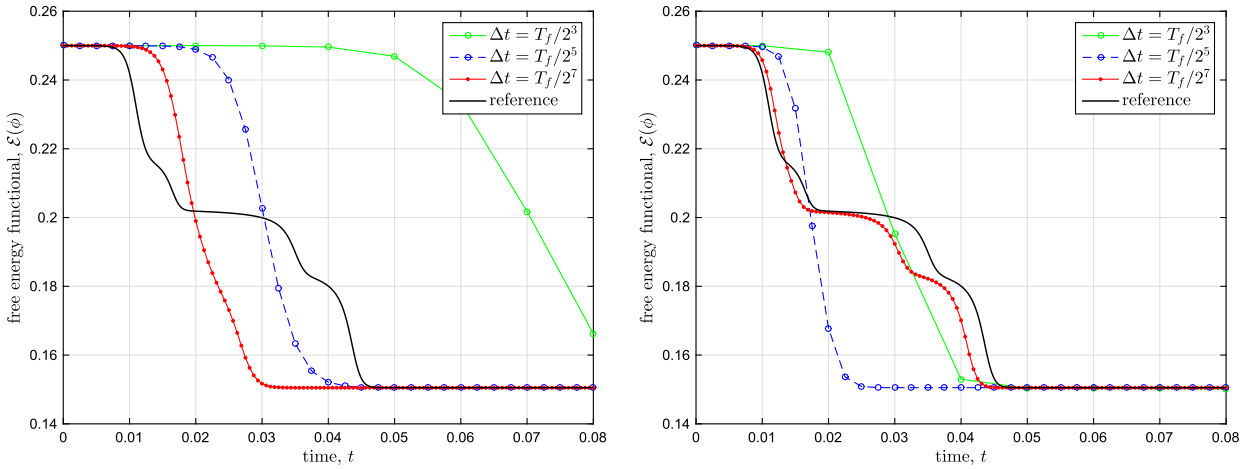

(a) CSRK-R(1) (b) CSRK-R(2)

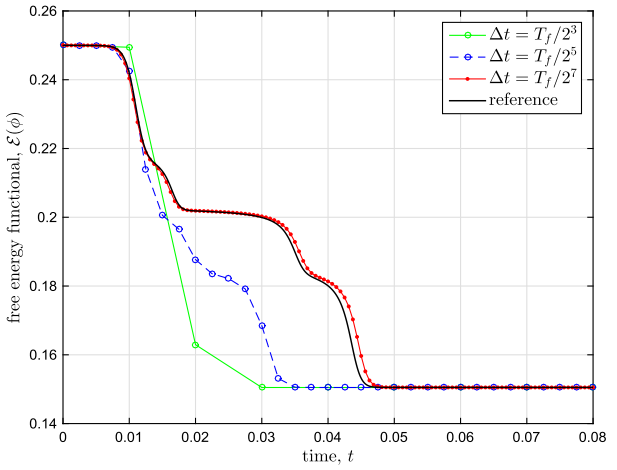

(c) CSRK-R(3)

Fig. 4. Energy evolution for the CH equation in 1D.

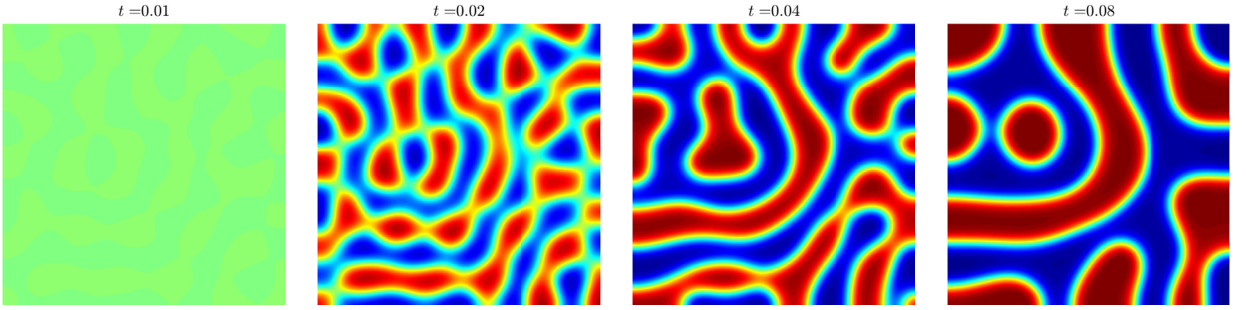

Fig. 5. Time evolution of solution for the CH equation in 2D. (For interpretation of the references to color in this figure, the reader is referred to the web version of this article.)

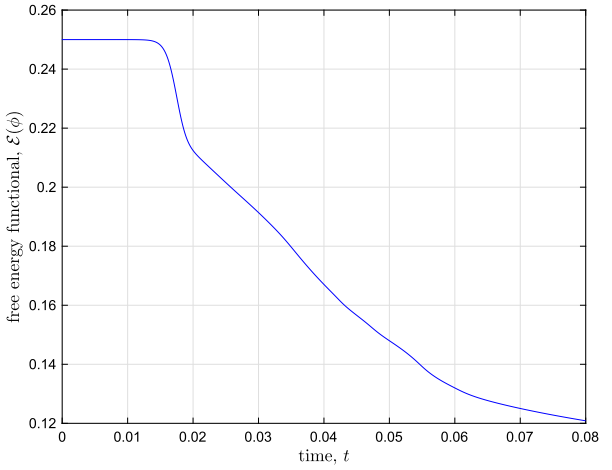

Fig. 6. Energy evolution for the CH equation in 2D.

Fig. 5 shows the time evolution of the solution with a sufficiently small time step $\Delta t = T_f/2^{17}$ using the third order method CSRK-R(3). In each figure, the red, green, and blue regions indicate $\phi = 1$, 0, -1, respectively. At the early stage, solutions are rearranged and adjusted to find their desired mode with low magnitude. After finishing the adjustment, the solution matures and merges. These solutions will be used as the reference solution to estimate the convergence rate in Section 5.6.

Fig. 6 shows the time evolution of free energy functional $\mathcal{E}(\phi)$ corresponding to the solution in Fig. 5. The property of the energy dissipation is validated and energy transitions are observed. The evolution will be used as the reference to compare with the energy evolution in Section 5.6.

5.5. Numerical convergence test with random initial data in 2D

We demonstrate the numerical convergence using the same conditions and parameters as those used in the previous section. To estimate the convergence rate with respect to a time step Δt, simulations are performed by varying the time steps $\Delta t = T_f/2^{15}, T_f/2^{14}, \ldots, T_f/2^3$.

Fig. 7 shows the relative l_2-errors of $\phi(x, y, t)$ with various time steps. Here, the errors are computed by comparison with the reference solution. It is observed that the CSRK-R(p) methods give the desired p-th order accuracy in time.

5.6. Energy stability performance with random initial data in 2D

We display the energy evolutions with the same conditions and parameters as those used in the previous section. Simulations are performed by relatively large time steps $\Delta t = T_f/2^7, T_f/2^5, T_f/2^3$.

Fig. 8 shows the energy evolution with large time steps and the energy dissipations are observed for all simulations.

5.7. Long-time evolution with random initial data in 2D

We display the long-time evolution using the same conditions and parameters as those used in the previous section except $T_f = 16$ and $\Delta t = 2^{-12}$. Here, we just provide a resolved computation for the long-time evolution with relatively

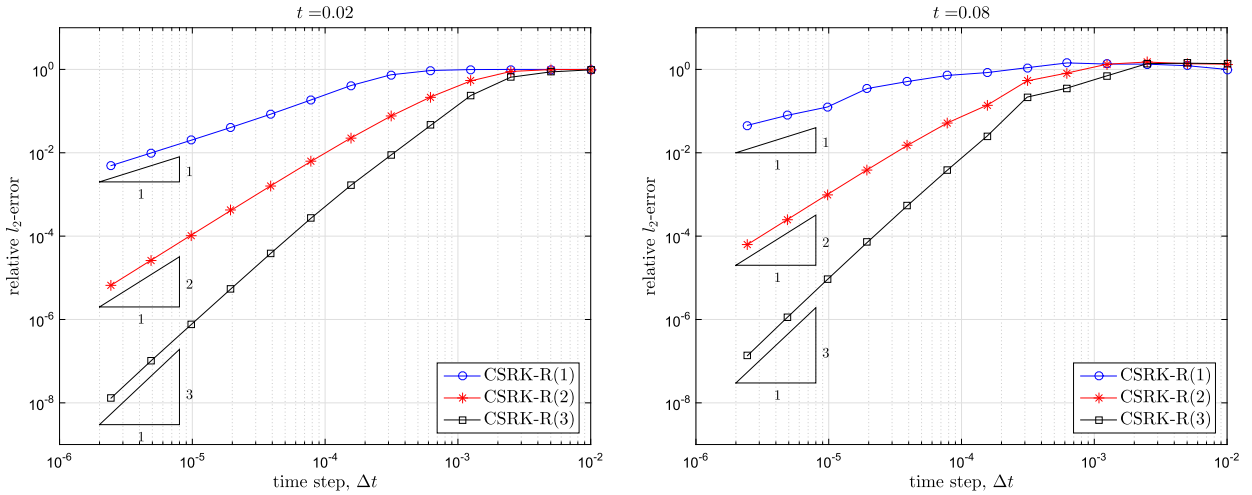

Fig. 7. Relative l_2-errors for various time steps Δt in 2D.

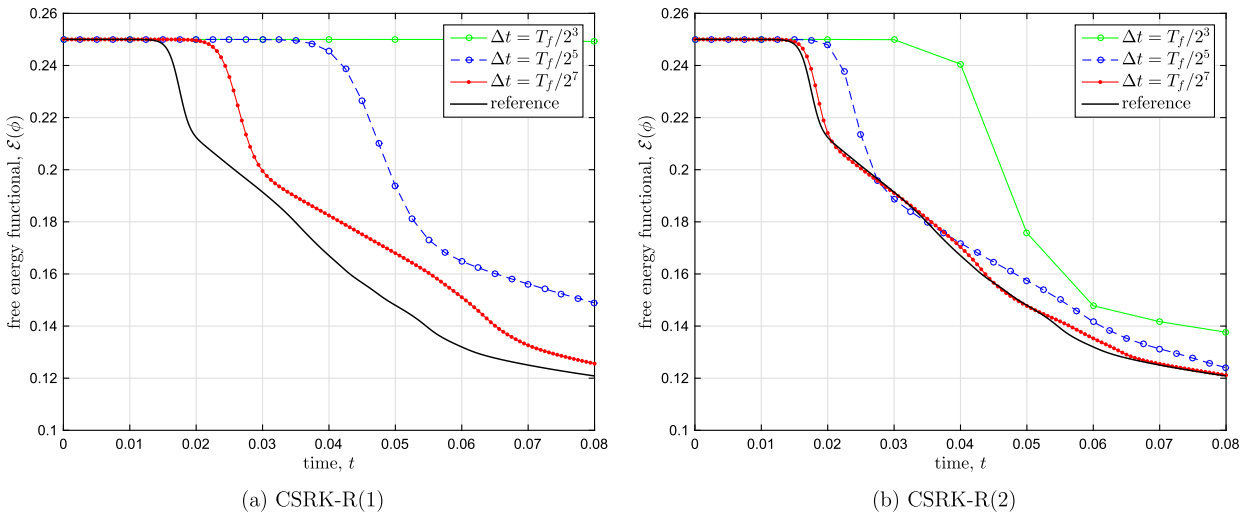

(a) CSRK-R(1) (b) CSRK-R(2)

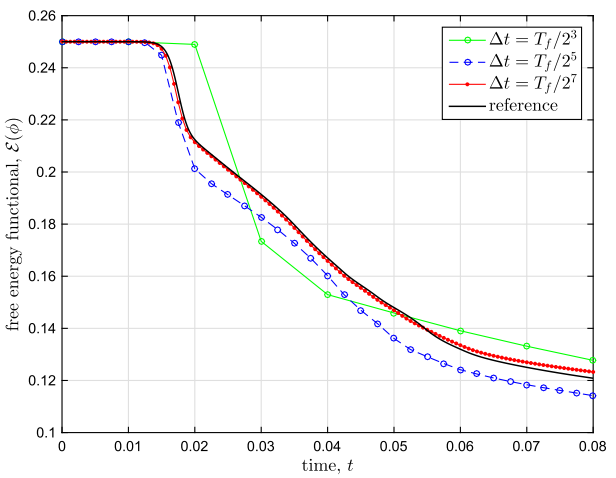

(c) CSRK-R(3)

Fig. 8. Energy evolution for the CH equation in 2D.

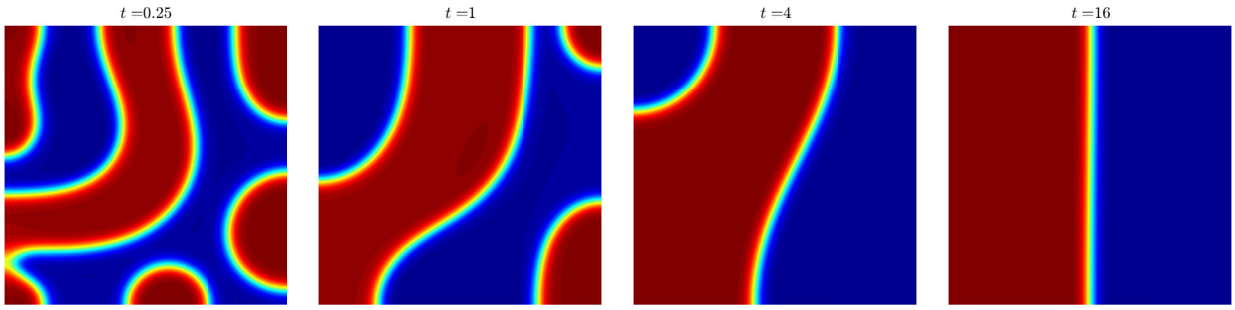

Fig. 9. Time evolution of solution for the CH equation in 2D. (For interpretation of the references to color in this figure, the reader is referred to the web version of this article.)

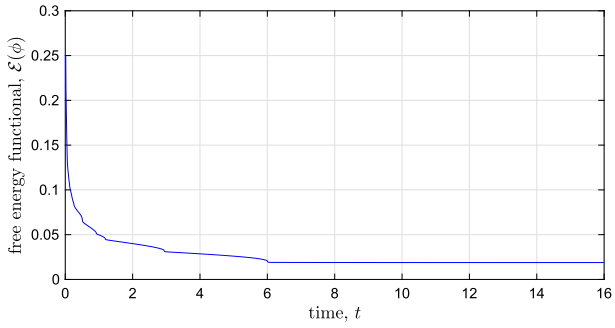

Fig. 10. Energy evolution for the CH equation in 2D.

smaller time step size and the interested readers can consider an algorithm such as an adaptive time stepping procedure to choose a bigger time step size.

Fig. 9 shows the time evolution of the solution using the third order method CSRK-R(3). In each figure, the red, green, and blue regions indicate $\phi = 1,\ 0,\ -1$, respectively. The coarsening is observed for long time and the solution finally approaches the steady state.

Fig. 10 shows the time evolution of free energy functional $\mathcal{E}(\phi)$ corresponding to the solution in Fig. 9.

6. Conclusions

We proposed unconditionally gradient stable methods to solve a gradient flow which is a fundamental concept in various dynamical systems. The main feature of the scheme is a combination of the convex splitting method and the multi-stage two-additive Runge–Kutta method with the resemble design. The proposed methods are high order accurate in time and assure unconditional gradient stability. In practical terms, we provided some examples of implicit–explicit Runge–Kutta type methods, which are not only unconditionally gradient stable but also uniquely solvable. Applying the proposed methods to the Cahn–Hilliard equation, we presented numerical experiments to show high order accuracy and unconditional gradient stability. We demonstrated the existence of the third order and energy stable method by presenting the specific examples. In future, we need to study what are optimal choices among the proposed methods and compare with the existing numerical methods in terms of numerical convergence error.

Acknowledgements

This research was supported by the Basic Science Research Program through the National Research Foundation of Korea (NRF), funded by the Korean Government MOE (2009-0093827) and MSIP (2015-003037, 2017R1D1A1B0-3032422, 2017R1D1A1B0-3034619).

Appendix A. Order conditions for two-additive Runge–Kutta method

Although could refer to [23,25,26,31] for information on the derivation and list of the order conditions, in this appendix, we briefly introduce the order conditions of a two-additive Runge–Kutta method to provide definite notations and information. The two-additively partitioned system

$$\frac{\partial \phi}{\partial t} = f(\phi) + g(\phi) \text{ and } \phi(0) = \phi^0, \tag{45}$$

Table 2
Order conditions of two-additive RK methods up to the third order accuracy. Here, we define the component-wise product as $\mathbf{x}\odot\mathbf{y}=(x_0y_0,x_1y_1,\ldots,x_sy_s)^T$ for $\mathbf{x}=(x_0,x_1,\ldots,x_s)^T$ and $\mathbf{y}=(y_0,y_1,\ldots,y_s)^T$, and $\mathbf{x}^m=\mathbf{x}\odot\mathbf{x}^{m-1}$ for $m>1$.

Order	Stand-alone conditions		Coupling conditions
1	$\mathbf{b}\cdot\mathbf{1}=1$	$\hat{\mathbf{b}}\cdot\mathbf{1}=1$	–
2	$\mathbf{b}\cdot\mathbf{c}=1/2$	$\hat{\mathbf{b}}\cdot\hat{\mathbf{c}}=1/2$	$\mathbf{b}\cdot\hat{\mathbf{c}}=\hat{\mathbf{b}}\cdot\mathbf{c}=1/2$ $\hat{\mathbf{b}}\cdot\mathbf{c}^2=\mathbf{b}\cdot\hat{\mathbf{c}}^2=1/3$
3	$\mathbf{b}\cdot\mathbf{c}^2=1/3$ $\mathbf{b}\cdot\mathbf{Ac}=1/6$	$\hat{\mathbf{b}}\cdot\hat{\mathbf{c}}^2=1/3$ $\hat{\mathbf{b}}\cdot\hat{\mathbf{A}}\hat{\mathbf{c}}=1/6$	$\hat{\mathbf{b}}\cdot(\mathbf{c}\odot\hat{\mathbf{c}})=\mathbf{b}\cdot(\mathbf{c}\odot\hat{\mathbf{c}})=1/3$ $\mathbf{b}\cdot\mathbf{A}\hat{\mathbf{c}}=\hat{\mathbf{b}}\cdot\hat{\mathbf{A}}\mathbf{c}=1/6$ $\mathbf{b}\cdot\hat{\mathbf{A}}\mathbf{c}+\hat{\mathbf{b}}\cdot\mathbf{Ac}=1/3$ $\mathbf{b}\cdot\hat{\mathbf{A}}\hat{\mathbf{c}}+\hat{\mathbf{b}}\cdot\mathbf{A}\hat{\mathbf{c}}=1/3$

is applied using two different Runge–Kutta (RK) methods for each $f(\phi)$ and $g(\phi)$. We denote two s-stage RK tables in the usual Butcher notation

$$\begin{array}{c|c}\mathbf{c}&\mathbf{A}\\\hline&\mathbf{b}^T\end{array}=\begin{array}{c|cccccc}0&0&0&0&\cdots&0\\c_1&a_{10}&a_{11}&a_{12}&\cdots&a_{1s}\\c_2&a_{20}&a_{21}&a_{22}&\cdots&a_{2s}\\\vdots&\vdots&\vdots&\vdots&\ddots&\vdots\\c_s&a_{s0}&a_{s1}&a_{s2}&\cdots&a_{ss}\\\hline&b_0&b_1&b_2&\cdots&b_s\end{array},\quad \begin{array}{c|c}\hat{\mathbf{c}}&\hat{\mathbf{A}}\\\hline&\hat{\mathbf{b}}^T\end{array}=\begin{array}{c|cccccc}0&0&0&0&\cdots&0\\\hat{c}_1&\hat{a}_{10}&\hat{a}_{11}&\hat{a}_{12}&\cdots&\hat{a}_{1s}\\\hat{c}_2&\hat{a}_{20}&\hat{a}_{21}&\hat{a}_{22}&\cdots&\hat{a}_{2s}\\\vdots&\vdots&\vdots&\vdots&\ddots&\vdots\\\hat{c}_s&\hat{a}_{s0}&\hat{a}_{s1}&\hat{a}_{s2}&\cdots&\hat{a}_{ss}\\\hline&\hat{b}_0&\hat{b}_1&\hat{b}_2&\cdots&\hat{b}_s\end{array}. \tag{46}$$

where $\mathbf{A},\hat{\mathbf{A}}\in\mathbb{R}^{(s+1)\times(s+1)}$ and $\mathbf{b},\hat{\mathbf{b}}\in\mathbb{R}^{s+1}$. Here, the coefficients $\mathbf{c}$ and $\hat{\mathbf{c}}$ are given by the usual relation $\mathbf{c}=\mathbf{A1}$ and $\hat{\mathbf{c}}=\hat{\mathbf{A}}\mathbf{1}$, respectively, where $\mathbf{1}=(1,1,\ldots,1)^T\in\mathbb{R}^{s+1}$.

We denote ϕ^n as an approximation of $\phi(t^n)$. Given ϕ^n, we calculate a next time approximation ϕ^{n+1} at $t^{n+1}=t^n+\Delta t$ with the intermediate stages, $\phi_0,\phi_1,\cdots,\phi_s$. We set a zero-stage as $k_0=f(\phi_0)$ and $\hat{k}_0=g(\phi_0)$, where $\phi_0=\phi^n$. For each stage $i=1,2,\ldots,s$, we calculate

$$k_i=f(\phi_i),\ \hat{k}_i=g(\phi_i),\ \text{where}\ \phi_i=\phi_0+\Delta t\left(\sum_{j=0}^{s}a_{ij}k_j+\sum_{j=0}^{s}\hat{a}_{ij}\hat{k}_j\right). \tag{47}$$

Here, ϕ_i is the approximation of $\phi(t^n+c_i\Delta t)$ on the i-th stage. For a vector notation $\boldsymbol{\phi}=(\phi_0,\phi_1,\ldots,\phi_s)^T$, we define the function evaluation as

$$f(\boldsymbol{\phi})=(f(\phi_0),f(\phi_1),\cdots,f(\phi_s))^T. \tag{48}$$

Now, we can respectively rewrite $\mathbf{k}=(k_0,k_1,\ldots,k_s)^T$ and $\hat{\mathbf{k}}=\left(\hat{k}_0,\hat{k}_1,\ldots,\hat{k}_s\right)^T$ as

$$\mathbf{k}=f\left(\phi_0\mathbf{1}+\Delta t\left(\mathbf{Ak}+\hat{\mathbf{A}}\hat{\mathbf{k}}\right)\right),\quad \hat{\mathbf{k}}=g\left(\phi_0\mathbf{1}+\Delta t\left(\mathbf{Ak}+\hat{\mathbf{A}}\hat{\mathbf{k}}\right)\right). \tag{49}$$

We also evaluate the next time approximation ϕ^{n+1} as

$$\phi^{n+1}=\phi_0+\Delta t\sum_{j=0}^{s}\left(b_jk_j+\hat{b}_j\hat{k}_j\right), \tag{50}$$

and it can be written as $\phi^{n+1}=\phi_0+\Delta t\left(\mathbf{b}\cdot\mathbf{k}+\hat{\mathbf{b}}\cdot\hat{\mathbf{k}}\right)$.

Table 2 lists the order conditions for (46) to have the first, second, and third order accuracy in time. A simple description of the order conditions is presented in [23], in which the Taylor's expansion only is used. For other explanations of the order condition, refer to [25,26,31] and references therein.

References

[1] J.K. Hale, Asymptotic Behavior of Dissipative Systems, American Mathematical Society, Providence, RI, 1988.
[2] S.M. Allen, J.W. Cahn, A microscopic theory for antiphase boundary motion and its application to antiphase domain coarsening, Acta Metall. 27 (6) (1979) 1085–1095.
[3] J.W. Cahn, J.E. Hilliard, Free energy of a nonuniform system. I. Interfacial free energy, J. Chem. Phys. 28 (2) (1958) 258–267.
[4] A.M. Stuart, A.R. Humphries, Model problems in numerical stability theory for initial value problems, SIAM Rev. 36 (2) (1994) 226–257.
[5] C.M. Elliott, A. Stuart, The global dynamics of discrete semilinear parabolic equations, SIAM J. Numer. Anal. 30 (6) (1993) 1622–1663.
[6] D.J. Eyre, An unconditionally stable one-step scheme for gradient systems, Unpublished article.

[7] J. Shen, X. Yang, Numerical approximations of Allen–Cahn and Cahn–Hilliard equations, Discrete Contin. Dyn. Syst. 28 (4) (2010) 1669–1691.
[8] D. Furihata, A stable and conservative finite difference scheme for the Cahn–Hilliard equation, Numer. Math. 87 (4) (2001) 675–699.
[9] J. Kim, A numerical method for the Cahn–Hilliard equation with a variable mobility, Commun. Nonlinear Sci. Numer. Simul. 12 (8) (2007) 1560–1571.
[10] L. Cueto-Felgueroso, J. Peraire, A time-adaptive finite volume method for the Cahn–Hilliard and Kuramoto–Sivashinsky equations, J. Comput. Phys. 227 (24) (2008) 9985–10017.
[11] X. Feng, T. Tang, J. Yang, Long time numerical simulations for phase-field problems using p-adaptive spectral deferred correction methods, SIAM J. Sci. Comput. 37 (1) (2015) A271–A294.
[12] X. Wu, G. Zwieten, K. Zee, Stabilized second-order convex splitting schemes for Cahn–Hilliard models with application to diffuse-interface tumor-growth models, Int. J. Numer. Methods Biomed. Eng. 30 (2) (2014) 180–203.
[13] J. Guo, C. Wang, S.M. Wise, X. Yue, An H^2 convergence of a second-order convex-splitting, finite difference scheme for the three-dimensional Cahn–Hilliard equation, Commun. Math. Sci. 14 (2) (2016) 489–515.
[14] Z. Hu, S.M. Wise, C. Wang, J.S. Lowengrub, Stable and efficient finite-difference nonlinear-multigrid schemes for the phase field crystal equation, J. Comput. Phys. 228 (15) (2009) 5323–5339.
[15] P. Vignal, L. Dalcin, D.L. Brown, N. Collier, V.M. Calo, An energy-stable convex splitting for the phase-field crystal equation, Comput. Struct. 158 (1) (2015) 355–368.
[16] J. Shin, H.G. Lee, J.-Y. Lee, First and second order numerical methods based on a new convex splitting for phase-field crystal equation, J. Comput. Phys. 327 (2016) 519–542.
[17] A. Baskaran, Z. Hu, J.S. Lowengrub, C. Wang, S.M. Wise, P. Zhou, Energy stable and efficient finite-difference nonlinear multigrid schemes for the modified phase field crystal equation, J. Comput. Phys. 250 (2013) 270–292.
[18] J. Shen, C. Wang, X. Wang, S.M. Wise, Second-order convex splitting schemes for gradient flows with Ehrlich–Schwoebel type energy: application to thin film epitaxy, SIAM J. Numer. Anal. 50 (1) (2012) 105–125.
[19] X. Yang, J. Zhao, Q. Wang, Numerical approximations for the molecular beam epitaxial growth model based on the invariant energy quadratization method, J. Comput. Phys. 333 (2017) 104–127.
[20] X. Yang, Linear, first and second-order, unconditionally energy stable numerical schemes for the phase field model of homopolymer blends, J. Comput. Phys. 327 (2016) 294–316.
[21] H. Gomez, T.J. Hughes, Provably unconditionally stable, second-order time-accurate, mixed variational methods for phase-field models, J. Comput. Phys. 230 (13) (2011) 5310–5327.
[22] P. Galenko, H. Gomez, N. Kropotin, K. Elder, Unconditionally stable method and numerical solution of the hyperbolic phase-field crystal equation, Phys. Rev. E 88 (1) (2013) 013310.
[23] J. Shin, H.G. Lee, J.-Y. Lee, Convex Splitting Runge–Kutta methods for phase-field models, Comput. Math. Appl. 73 (11) (2017) 2388–2403.
[24] U.M. Ascher, S.J. Ruuth, R.J. Spiteri, Implicit–explicit Runge–Kutta methods for time-dependent partial differential equations, Appl. Numer. Math. 25 (2–3) (1997) 151–167.
[25] C. Kennedy, M. Carpenter, Additive Runge–Kutta schemes for convection–diffusion–reaction equations, Appl. Numer. Math. 44 (1–2) (2003) 139–181.
[26] E. Zharovsky, A. Sandu, H. Zhang, A class of implicit–explicit two-step Runge–Kutta methods, SIAM J. Numer. Anal. 53 (1) (2015) 321–341.
[27] E. Hairer, G. Wanner, Solving Ordinary Differential Equations II, vol. 14, Springer-Verlag, Berlin, 1996.
[28] R. Alexander, Diagonally implicit Runge–Kutta methods for stiff ODE's, SIAM J. Numer. Anal. 14 (6) (1977) 1006–1021.
[29] D.J. Eyre, Unconditionally gradient stable time marching the Cahn–Hilliard equation, in: MRS Proceedings, vol. 529, Cambridge Univ. Press, 1998, p. 39.
[30] H.G. Lee, J. Shin, J.-Y. Lee, First and second order operator splitting methods for the phase field crystal equation, J. Comput. Phys. 299 (2015) 82–91.
[31] L. Pareschi, G. Russo, Implicit–explicit Runge–Kutta schemes for stiff systems of differential equations, Recent Trends Numer. Anal. 3 (2000) 269–289.